Small-Molecule Stabilization of 14-3-3 Protein-Protein Interactions Stimulates Axon Regeneration

Highlights

- 14-3-3 adaptor proteins facilitate axon growth

- Stabilization of 14-3-3 complexes with Fusicoccin-A stimulates axon regeneration

- Fusicoccin-A targets a complex between 14-3-3 and the stress response regulator GCN1

- GCN1 acts as an intrinsic brake on neurite outgrowth

Authors

Andrew Kaplan, Barbara Morquette, Antje Kroner, ..., Nicolas Bisson, Samuel David, Alyson E. Fournier

Correspondence

alyson.fournier@mcgill.ca

In Brief

Kaplan et al. describe a novel pharmacological strategy with a unique mechanism of action to enhance axon regeneration in the injured CNS. Fusicoccin-A stabilizes 14-3-3 protein complexes and stimulates nerve regeneration, in part through modulation of the stress response regulator GCN1.

Small-Molecule Stabilization of 14-3-3 Protein-Protein Interactions Stimulates Axon Regeneration

Andrew Kaplan,[1] Barbara Morquette,[1] Antje Kroner,[2,5] SooYuen Leong,[1] Carolin Madwar,[3] Ricardo Sanz,[1] Sara L. Banerjee,[4] Jack Antel,[1] Nicolas Bisson,[4] Samuel David,[5] and Alyson E. Fournier[1,6,*]

[1]Department of Neurology and Neurosurgery, Montréal Neurological Institute, McGill University, Montréal, QC H3A 2B4, Canada
[2]Department of Neurosurgery, Medical College of Wisconsin, VA Medical Center, Milwaukee, WI 53295, USA
[3]Department of Chemistry, McGill University, Montréal, QC H3A 0B8, Canada
[4]Département de Biologie Moléculaire, Biochimie Médicale et Pathologie, and Centre de Recherche sur le Cancer, Université Laval, Québec City, QC G1V 0A6, Canada
[5]Centre for Research in Neuroscience, The Research Institute of the McGill University Health Centre, Montréal, QC H3G 1A4, Canada
[6]Lead Contact
*Correspondence: alyson.fournier@mcgill.ca
http://dx.doi.org/10.1016/j.neuron.2017.02.018

SUMMARY

Damaged central nervous system (CNS) neurons have a poor ability to spontaneously regenerate, causing persistent functional deficits after injury. Therapies that stimulate axon growth are needed to repair CNS damage. 14-3-3 adaptors are hub proteins that are attractive targets to manipulate cell signaling. We identify a positive role for 14-3-3s in axon growth and uncover a developmental regulation of the phosphorylation and function of 14-3-3s. We show that fusicoccin-A (FC-A), a small-molecule stabilizer of 14-3-3 protein-protein interactions, stimulates axon growth in vitro and regeneration in vivo. We show that FC-A stabilizes a complex between 14-3-3 and the stress response regulator GCN1, inducing GCN1 turnover and neurite outgrowth. These findings show that 14-3-3 adaptor protein complexes are druggable targets and identify a new class of small molecules that may be further optimized for the repair of CNS damage.

INTRODUCTION

Neurons in the central nervous system (CNS) have a poor capacity to spontaneously repair after injury, limiting restitution of motor and sensory function. Stimulation of axon growth is an important strategy to encourage repair of damaged connections. Robust axon regeneration after injury can be elicited by genetic manipulation of oncogenes and tumor suppressors (Belin et al., 2015; O'Donovan et al., 2014; Park et al., 2008; Sun et al., 2011). These studies have suggested that a global alteration of the cell-intrinsic growth state is required to achieve extensive axon regeneration. However, the current challenge is to identify druggable targets and treatments to repair CNS injury.

Adaptor proteins facilitate many important molecular processes and are interesting targets to manipulate the intrinsic growth state. 14-3-3s are a seven-isoform (β, γ, ε, ζ, η, θ, σ) family of dimeric cytosolic adaptor proteins highly expressed in the CNS. 14-3-3s have pervasive roles in cell signaling and are important regulators of neurodevelopment and axon guidance (Cheah et al., 2012; Kent et al., 2010; Toyo-oka et al., 2003, 2014; Yam et al., 2012); however, their roles in axon growth and regeneration after injury are unknown. Here we report that 14-3-3s enhance axon growth. Moreover, we find that a developmental increase in 14-3-3 phosphorylation antagonizes 14-3-3 function.

14-3-3s bind to serine- and threonine-phosphorylated client proteins via a highly conserved binding groove (Figure 1A). Intriguingly, a small molecule called fusicoccin-A (FC-A) can be used as a chemical tool to stabilize 14-3-3:client complexes. FC-A binds to a solvent-exposed hydrophobic pocket created by the interface of the 14-3-3 binding groove and certain client proteins (de Boer and de Vries-van Leeuwen, 2012). Pharmacological stabilization of 14-3-3 PPIs is a potentially powerful approach to alter the cell-intrinsic growth state through modulation of multiple signaling pathways. We discover that FC-A stimulates neurite outgrowth in vitro, reduces corticospinal axon dieback after spinal cord injury, and stimulates optic nerve regeneration. We demonstrate that FC-A acts through a 14-3-3-dependent mechanism and identify FC-A-binding proteins using bead-immobilized FC-A and mass spectrometry. We show that FC-A stabilizes a complex between 14-3-3 and the stress response regulator GCN1, leading to GCN1 turnover and enhanced neurite outgrowth. These results identify a novel strategy and class of small molecules to enhance axon growth after injury.

RESULTS

14-3-3s Promote Neurite Outgrowth and Axon Regeneration In Vitro

To assess the role of 14-3-3 adaptor proteins in neurite outgrowth, we treated embryonic day 18 (E18) rat cortical neurons with BV02,
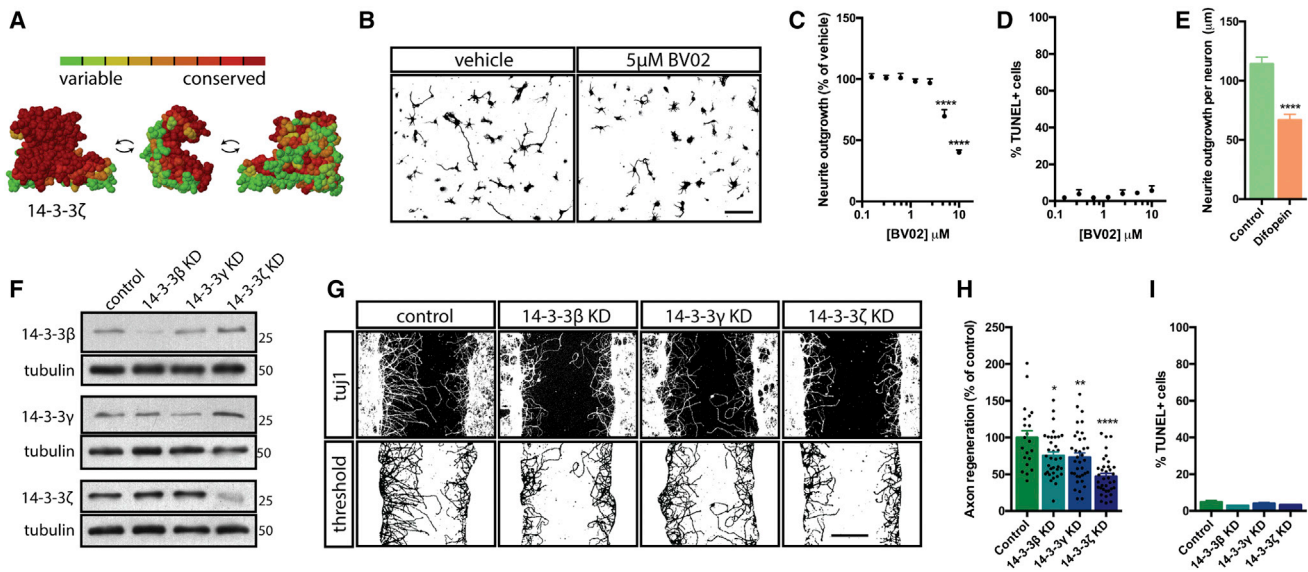
Figure 1. 14-3-3 Loss of Function Impairs Neurite Outgrowth and Regeneration In Vitro

(A) Crystal structure of human 14-3-3ζ (PDB: 4HKC) color-coded for evolutionary sequence conservation using ConSurf.

(B–D) Treatment of E18 rat cortical neurons with BV02 small molecule 14-3-3 inhibitor reduces neurite outgrowth (B and C) and does not induce apoptosis (D) (n = 3, ****p < 0.0001 Fisher's LSD, scale bar = 100 μm).

(E) Expression of dimeric R18 (difopein) impairs neurite outgrowth (n = 60 neurons from 3 experiments, ****p < 0.0001, t test).

(F–I) Knockdown of 14-3-3 β, γ, ζ (F) impairs axon regeneration (G and H) and does not induce apoptosis after scratch injury (I) (n = 21–36 scratches from 3 experiments, *p < 0.05, **p < 0.01, ***p < 0.001, one-way ANOVA Dunnett's post-test, scale bar = 200 μm). Data are presented as mean + SEM.

a cell-permeable small molecule inhibitor of 14-3-3 PPIs (Corradi et al., 2010; Gómez-Suárez et al., 2016; Mohammad et al., 2013). BV02 significantly reduced neurite growth at low micromolar concentrations and at 10 μM many of the neurons failed to initiate neurites or only sprouted few very short processes, with an overall ∼60% reduction in average total neurite length per neuron (Figures 1B and 1C). This was not accompanied by any significant increase in TUNEL-positive apoptotic cells (Figure 1D). Expression of dimeric R18 (difopein), a peptide inhibitor of 14-3-3s (Masters and Fu, 2001), similarly impaired neurite outgrowth (Figure 1E). We next investigated the effect of knocking down individual 14-3-3 isoforms on axon regeneration in vitro. We employed a scratch assay where rat cortical neurons are grown to confluence for 10 days and mechanically injured with a pipet tip (Huebner et al., 2011). The day after injury, nearly all the regenerating neurites are tau-positive axons (Figure S1A). 14-3-3s are present throughout the soma and neurites in mature sparse cultures (Figure S1B); however, there is an enrichment at the growth cone tips after scratch injury, suggesting a role in axon regrowth (arrowheads, Figure S1C). Knockdown of 14-3-3 isoforms β, γ, or ζ significantly reduced axon regeneration after scratch injury (Figures 1F–1H) and did not impact cell survival (Figure 1I). We confirmed the specificity of these effects in a neurite outgrowth assay by expressing RNAi-resistant myc-tagged 14-3-3s and found that this was sufficient to restore baseline levels of growth (Figure S2). Further supporting a positive role for 14-3-3s in axon growth, overexpression of myc-tagged 14-3-3 β, γ, or ζ significantly enhanced regeneration after scratch injury (Figures 2A–2C).

Phosphorylated 14-3-3 Is Elevated in Adulthood and Fails to Promote Neurite Outgrowth

Phosphorylation of a conserved serine (S58) in the 14-3-3 dimerization interface impairs dimerization and binding to client proteins (Powell et al., 2003; Shen et al., 2003; Woodcock et al., 2003; Zhou et al., 2009). Intriguingly, we found that 14-3-3 phosphorylation in the cortex is upregulated between the second and third week of life and high levels persist into adulthood (Figures 2D and 2E). We tested the effect of 14-3-3 phosphorylation on neurite outgrowth and found that overexpression of both wild-type 14-3-3ζ and a non-phosphorylatable S58A mutant enhanced neurite outgrowth, while overexpression of a phosphomimetic S58E mutant was ineffective (Figures 2F and 2G). We also found that overexpressed 14-3-3 is largely unphosphorylated relative to endogenous 14-3-3 (arrowheads, Figure 2H), suggesting that the process mediating 14-3-3 phosphorylation is saturated. Together, this supports a model wherein an increase in phosphorylation-mediated antagonism of 14-3-3 function contributes to a decline in the intrinsic capacity of neurons to grow.

Fusicoccin-A, a Small-Molecule Stabilizer of 14-3-3 PPIs, Enhances Neurite Outgrowth and Improves Axon Regeneration In Vitro

Fusicoccin-A (FC-A) is a fusicoccane small molecule produced by the *Phomopsis amygdali* fungus that stabilizes the binding between 14-3-3s and client proteins (de Boer and de Vries-van Leeuwen, 2012). Crystal structures of FC-A bound to 14-3-3:client complexes show that FC-A binds to a pocket created by the interface of the 14-3-3 binding groove and the
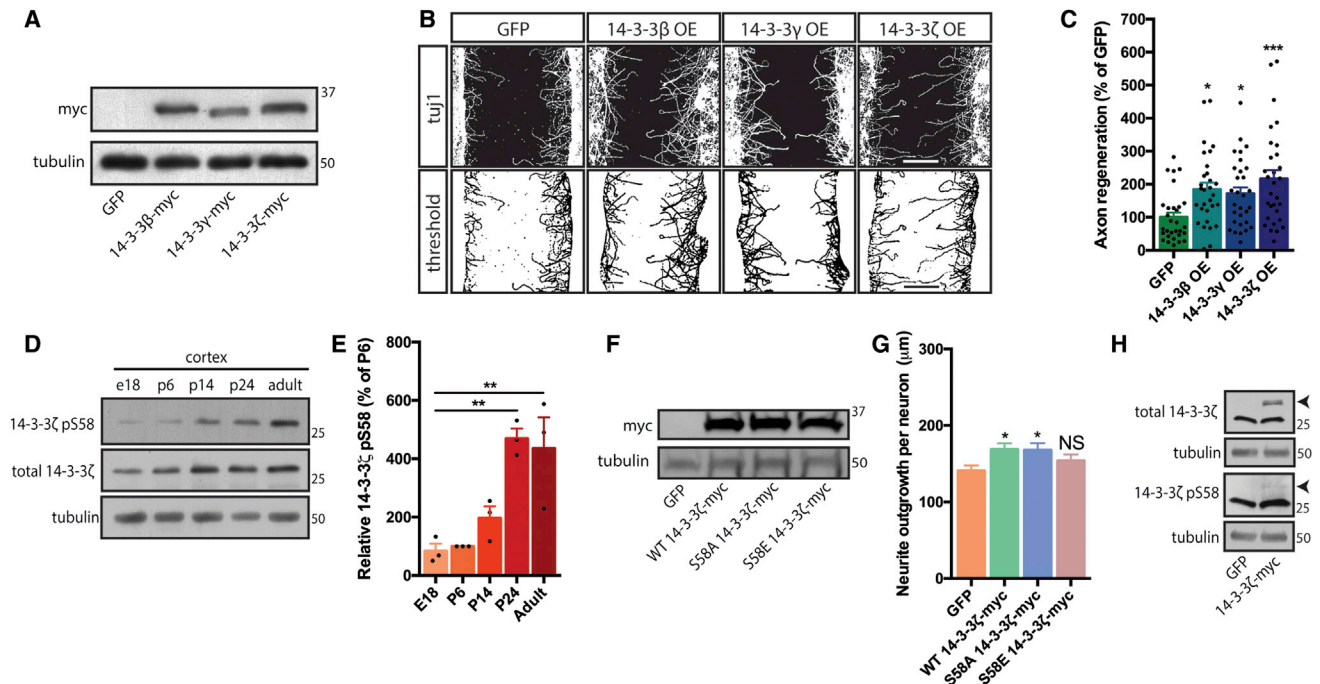
Figure 2. 14-3-3 Overexpression Enhances Axon Regeneration In Vitro

(A) Western blot of overexpressed myc-tagged 14-3-3 β, γ, ζ in cortical neurons.

(B and C) 14-3-3 overexpression (OE) in scratch injured cortical neurons (scale bar = 200 μm) (B) enhances axon regeneration (C) (n = 30 scratches from 3 experiments, *p < 0.05, ***p < 0.001, one-way ANOVA Dunnett's post-test).

(D and E) Western blots from cortex of different developmental stages (D) and densitometry of 14-3-3ζ pS58 normalized to P6 total 14-3-3ζ and tubulin (E) (n = 3, **p < 0.01, one-way ANOVA Dunnett's post-test).

(F) Overexpression of myc-tagged wild-type, S58A, and S58E 14-3-3ζ.

(G) S58E 14-3-3ζ mutant fails to enhance neurite outgrowth (n = 69–74 neurons from 3 experiments, *p < 0.05, one-way ANOVA Dunnett's post-test). Data are presented as mean + SEM.

(H) Exogenously expressed 14-3-3ζ is largely unphosphorylated relative to endogenous 14-3-3ζ pS58 (arrowheads, overexpressed myc-14-3-3ζ).

client peptide docked within the groove (Würtele et al., 2003) (Figure 3A). FC-A has a very low affinity for "un-cliented" 14-3-3 and binds to a limited set of 14-3-3:client complexes, dependent on client motif sequences (Würtele et al., 2003). We reasoned that FC-A, by its ability to stabilize 14-3-3 PPIs, might be a means to pharmacologically harness the pro-growth activity of 14-3-3s in neurons. Treatment of cortical neurons with FC-A produced a striking dose-dependent enhancement of neurite outgrowth on day 1 of culture (Figures 3B and 3C). Stimulation of neurite outgrowth was apparent at low micromolar concentrations with an EC_{50} of 29 μM (Figure 3D). A maximal effect of more than doubling neurite outgrowth per cell was reached at ∼200 μM. The EC_{50} is comparable to biologically active concentrations of FC-A that have been reported in other mammalian cell types (Bury et al., 2013; Camoni et al., 2011; De Vries-van Leeuwen et al., 2013). FC-A also markedly enhanced axon regeneration after scratch injury (Figures 3E and 3F). Although no outward toxicity was noted, axon regeneration peaked at 25 μM and began to decline at higher doses, suggesting that injured aged cortical neurons may be more sensitive to high doses of FC-A. Importantly, FC-A also promoted outgrowth from primary human fetal neurons, indicating a conservation of activity from rodent to human (Figures 3G and 3H).

FC-A Requires 14-3-3 PPIs to Stimulate Neurite Outgrowth

To confirm that FC-A targets 14-3-3 s to induce neurite outgrowth, we treated cortical neurons with a combination of FC-A and the cell-permeable 14-3-3 PPI inhibitor BV02. FC-A failed to elicit a significant increase in neurite outgrowth in the presence of BV02, which severely impaired baseline neurite outgrowth as expected (Figures 4A and 4B). In parallel as a control, we cultured neurons in the presence of the rho kinase inhibitor Y-27632, a known neurite outgrowth inducer, and found that BV02 had no effect on the ability of Y-27632 to stimulate outgrowth (Figures 4A and 4B). Interestingly, although Y-27632 is more potent in the neurite outgrowth assay, it does not significantly stimulate regeneration after scratch injury of aged cultures, consistent with another report showing no effect of Y-27632 in the same scratch injury paradigm (Figure S3; Huebner et al., 2011). To further test the 14-3-3 dependence of FC-A-induced neurite outgrowth, we knocked down 14-3-3 β, γ, and ζ, which resulted in a substantial depletion of total 14-3-3 (Figure 4C). This significantly impaired FC-A-induced neurite outgrowth, further supporting that FC-A functions through a 14-3-3-dependent mechanism (Figure 4D). We have previously shown that 14-3-3s regulate axon guidance through
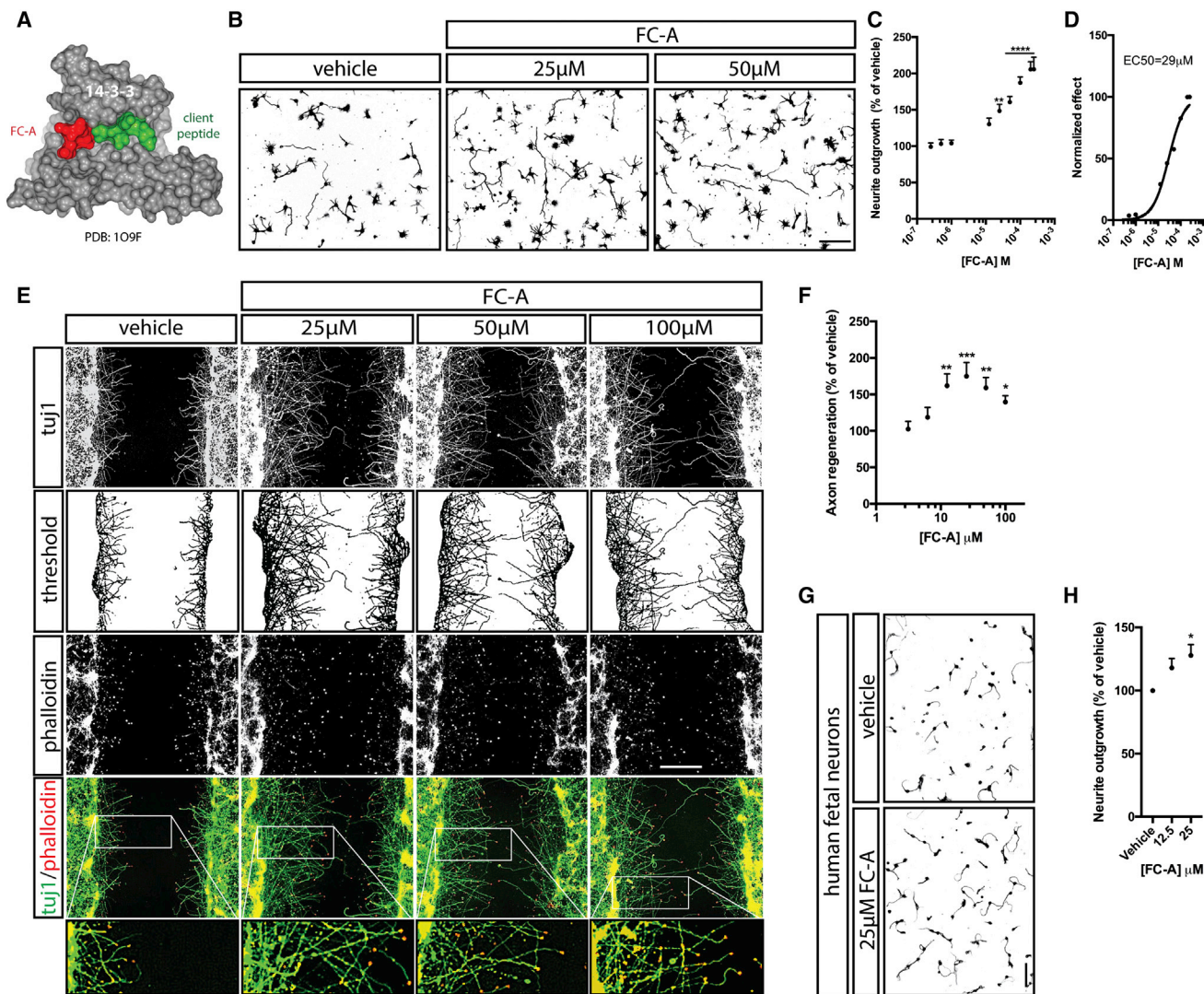
Figure 3. 14-3-3 Modulator Fusicoccin-A Enhances Neurite Outgrowth and Regeneration In Vitro

(A) Crystal structure of FC-A in ternary complex with 14-3-3 and a client peptide (PDB: 1O9F).

(B) FC-A stimulates neurite outgrowth from cortical neurons (scale bar = 100 μm).

(C) Dose response curve shows dose-dependence of FC-A stimulation of neurite outgrowth (n = 6, **p < 0.01, ****p < 0.0001, one-way ANOVA Fisher's LSD).

(D) Normalized dose-response curve reveals with an EC_{50} of 29 μM.

(E and F) FC-A enhances axon regeneration after scratch injury (E) in a dose-dependent manner (F) (n = 18 scratches from 3 experiments, **p < 0.01, ***p < 0.001, one-way ANOVA Fisher's LSD, scale bar = 200 μm).

(G and H) FC-A enhances neurite outgrowth from primary human fetal neurons (G) in a dose-dependent manner (H) (n = 3, *p < 0.05, one-way ANOVA Fisher's LSD, scale bar = 100 μm). Data are presented as mean +SEM.

modulation of protein kinase A (PKA) (Kent et al., 2010; Yam et al., 2012). However, inhibition of PKA with KT5720 had no effect on FC-A-induced neurite outgrowth (Figure S4), suggesting that FC-A stimulates neurite outgrowth in PKA-independent manner.

Identification of FC-A targets in Cortical Neurons

To identify FC-A targets, we chemically coupled FC-A to magnetic beads (Figure 4E) to use as an affinity reagent for pull-downs from cortical neuron lysate. We first confirmed that FC-A-beads selectively precipitate 14-3-3 proteins (Figure 4F).

Interestingly, FC-A beads precipitated a small fraction of total 14-3-3, suggesting a small pool of "cliented" 14-3-3s. The 14-3-3 PPI inhibitor R18, which spans the binding groove, blocked the binding of 14-3-3 to the beads, indicating that 14-3-3 binds to FC-A at the client-binding groove and not at another surface of the protein (Figure 4F). The client-binding-deficient phospho-S58 species was not precipitated by FC-A beads, again indicating that FC-A selectively binds cliented 14-3-3s (Figure 4G). As a control for binding specificity, soluble FC-A impaired 14-3-3 binding to the FC-A-beads (Figure 4H).
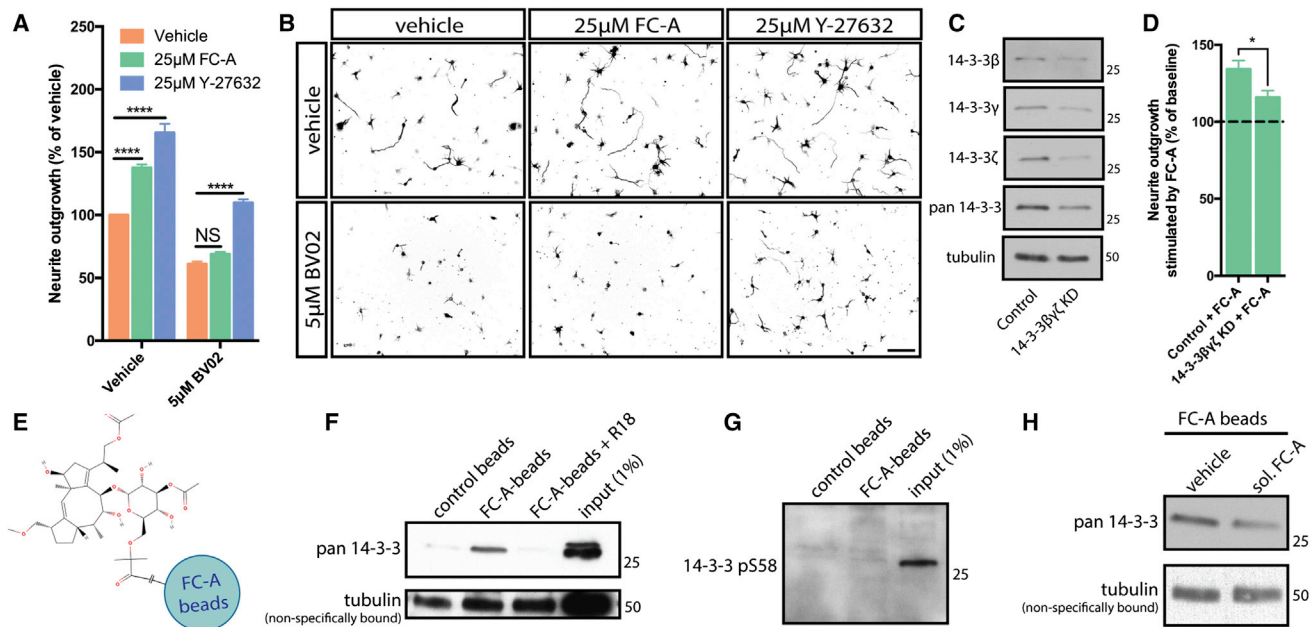
Figure 4. FC-A Binds to 14-3-3 Proteins in Neuron Lysate and Induces Neurite Outgrowth in a 14-3-3-Dependent Manner
(A) Inhibition of 14-3-3 s with BV02 blocks FC-A-induced stimulation of neurite outgrowth without affecting Y-27632-induced neurite outgrowth.
(B) Images of cortical neurons treated with drug combinations (n = 3, ****p < 0.0001, two-way ANOVA Bonferroni's post-test, scale bar = 100 μm).
(C) Western blot showing knockdown of 14-3-3 β, γ, and ζ.
(D) Knockdown of 14-3-3s impairs FC-A-induced outgrowth (n = 4, *p < 0.05, unpaired t test). Data are presented as mean + SEM.
(E) Coupling of FC-A to beads.
(F) FC-A-beads selectively precipitate 14-3-3s from cortical neuron lysate and R18 blocks binding.
(G) FC-A beads do not precipitate 14-3-3 pS58.
(H) Soluble FC-A blocks binding of 14-3-3 to FC-A-beads.

To gain insight into the mechanism underlying FC-A-induced neurite outgrowth, we used FC-A-beads for affinity chromatography followed by mass spectrometry to identify the complement of FC-A-binding proteins. Pull-downs from cortical neuron lysate using FC-A-beads or control beads were performed in three independent experiments. Using "significance analysis of interactome" (SAINT) (Choi et al., 2011), we identified 14 high-probability interactors (cutoff of 0.9). Remarkably, 13 of these 14 proteins contain potential FC-A/14-3-3 binding motifs (Table S1), defined by the characteristics of known binding motifs that can either be C-terminal serines or threonines (S/T) or internal S/T preceded by an arginine and followed by residues with small hydrophobic side chains. Of these proteins, "general control non-derepressible 1" (GCN1), a regulator of translation in response to cell stress, possesses 11 potential binding sites, one of which has identical sequence to a known binding site (Stevers et al., 2016). We therefore focused our efforts on querying a potential role for GCN1 in FC-A-dependent neurite outgrowth.

FC-A Stabilizes a GCN1:14-3-3 Complex and Induces GCN1 Turnover in Cortical Neurons

We first confirmed that FC-A-beads selectively precipitate GCN1 and that soluble FC-A blocks the interaction by western blot (Figures 5A and 5B). FC-A beads precipitated a relatively large proportion of GCN1 compared to 14-3-3, likely reflecting

the selective precipitation of a large pool of GCN1 that is incorporated into a relatively small pool of cliented 14-3-3s. Supporting this idea, R18 blocked the binding of GCN1 to the FC-A-beads, demonstrating the 14-3-3 dependence of FC-A binding to GCN1. Moreover, we immunoprecipitated GCN1 and found that FC-A stimulates the co-precipitation of 14-3-3 (Figure 5C). As 14-3-3s are known to sequester and affect the stability of client proteins (Tzivion et al., 2001), we assessed the effect of FC-A treatment on GCN1 expression in cortical neurons. Interestingly, we found a dose-dependent decrease in GCN1 expression levels (Figures 5D and 5E). 14-3-3s can mediate proteasome-dependent turnover of client proteins (Qureshi et al., 2013; Toyo-oka et al., 2014; Wang et al., 2010), so we therefore assessed the effect of proteasome inhibition with MG132. This increased GCN1 levels and attenuated the FC-A-mediated decrease, suggesting that FC-A induces proteasomal degradation of GCN1 potentially via stabilization of a GCN1:14-3-3 complex (Figures 5F and 5G).

GCN1 Loss of Function Contributes to FC-A-Induced Neurite Outgrowth

To determine whether loss of GCN1 underlies FC-A-induced neurite outgrowth, we electroporated cortical neurons with a GCN1-targeting shRNA together with GFP and cultured the neurons in the presence of vehicle or FC-A. Knockdown of GCN1 significantly enhanced basal neurite outgrowth (Figures 6A–6C). The
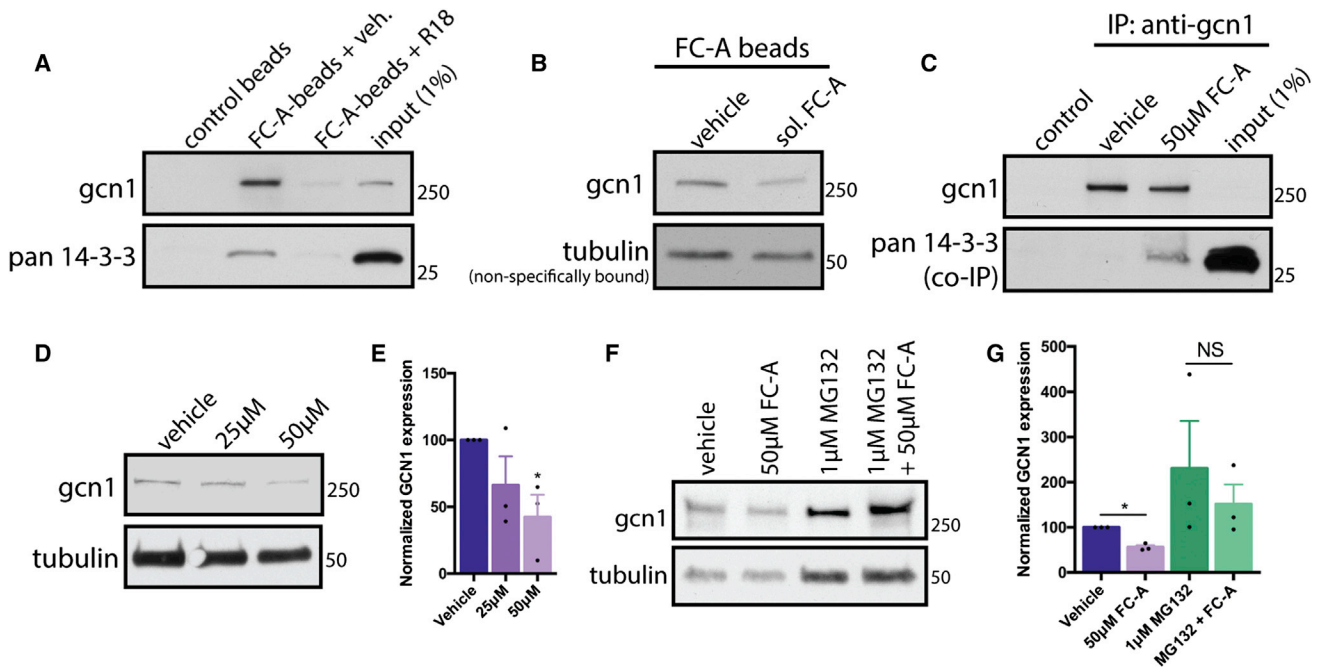
Figure 5. FC-A Binds to GCN1 in a 14-3-3-Dependent Manner and Induces GCN1 Turnover

(A) GCN1 selectively binds to FC-A-beads and R18 blocks binding.

(B) Soluble FC-A blocks the binding of GCN1 to FC-A-beads.

(C) FC-A induces a co-immunoprecipitation of 14-3-3 with GCN1.

(D and E) Western blot (D) and densitometry (E) showing that 24 hr treatment of cortical neurons with FC-A induces a dose-dependent decrease in GCN1 expression (n = 3, *p < 0.05, Fisher's LSD).

(F and G) Western blot (F) and densitometry (G) showing that co-treatment of cortical neurons with FC-A and the proteasome inhibitor MG132 attenuates FC-A-mediated GCN1 turnover (n = 3, *p < 0.05, one-way ANOVA Bonferroni's post-test). Data are presented as mean + SEM.

improved outgrowth of GCN1 knockdown neurons occluded any further enhancement by 25 μM FC-A, but the neurons did respond to a higher dose of 100 μM (Figure 5C). This indicates that FC-A acts in part through GCN1 loss of function, releasing an intrinsic "brake" on neurite outgrowth, but that other molecular pathways are also engaged by higher doses. Further supporting this model, 25 μM FC-A is also capable of stimulating neurite outgrowth from a population of neurons with more than ~100 μm baseline outgrowth (Figure 6D). GCN1 is solely known for its role in reducing global translation by binding and activating the eIF2α kinase GCN2 in response to cell stress. GCN2-dependent phosphorylation of the eIF2 subunit on a conserved serine (S51) converts eIF2 to a dominant negative, reducing global translation (Sattlegger and Hinnebusch, 2000). We therefore postulated that because FC-A reduces GCN1 expression, this might lead to an increase in global translation that could be responsible for stimulating neurite outgrowth. We treated neurons with a combination of 25 μM FC-A and cycloheximide (CHX) or anisomycin to block translation. Both CHX and anisomycin severely impaired neurite outgrowth but did not fully block the stimulation of neurite outgrowth by 25 μM FC-A (Figures 6E and 6F), suggesting a mechanism that may be independent from protein synthesis. Moreover, we found that FC-A does not have any reproducible effect on eIF2α phosphorylation (Figures 6G and 6H). Rapamycin also failed to block outgrowth induced by both FC-A and GCN1 knockdown (Figure S5), suggesting a mechanism independent

of mTOR, a well-established pro-regeneration pathway. Combined, these results indicate that 14-3-3 PPI stabilization with FC-A stimulates axon growth in part by stabilizing a 14-3-3: GCN1 complex, resulting in GCN1 downregulation (Figure 6I).

A Single Application of FC-A Reduces Corticospinal Axon Die-Back after Dorsal Hemisection Spinal Cord Injury

The damaged CNS is characterized by the presence of growth inhibitors including chondroitin sulfate proteoglycans (CSPGs) produced by reactive glia. FC-A significantly improved neurite outgrowth on aggrecan substrates, suggesting that it may be efficacious in improving growth after injury in vivo (Figure S6). We therefore sought to determine whether FC-A could improve axon growth after a dorsal hemisection spinal cord injury, which transects the entire corticospinal tract (CST). Mice received an immediate local application of FC-A in a rapidly polymerizing fibrin gel onto the injury site. CST axons were then anterogradely traced by injecting biotinylated dextran amine (BDA) into the motor cortex and the mice were analyzed on day 21 (Figure 7A). Surgeries and analysis were performed blinded to the experimental condition in two independent cohorts. Mice that received a single treatment of FC-A had a significant reduction in axonal die-back away from the injury site compared to control mice treated with vehicle-containing fibrin gel. While the cut axons of control mice retracted an average distance of ~72 μm, the
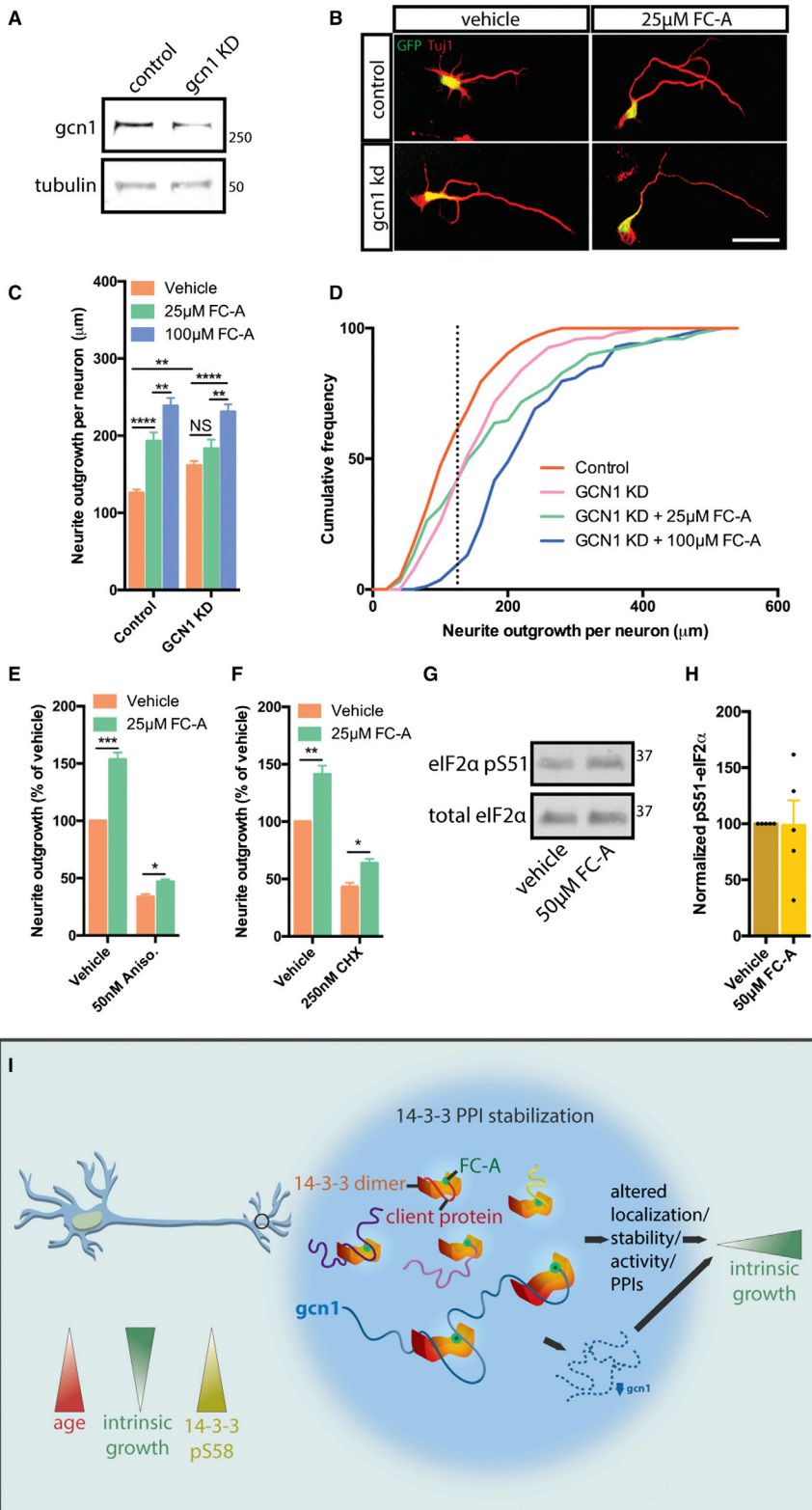
Figure 6. GCN1 Knockdown Enhances Neurite Outgrowth and Contributes to FC-A-Dependent Growth

(A–C) Knockdown of GCN1 in cortical neurons (A) enhances baseline neurite outgrowth and blocks a further increase in outgrowth induced by 25 μM FC-A but not by 100 μM FC-A (B and C) (scale bar = 50 μm).

(D) Cumulative frequency distribution of neurite outgrowth, dashed line indicates separation of GCN1 KD and 25 μM FC-A curves (n = 84–163 neurons, **p < 0.01, ****p < 0.0001, two-way ANOVA Tukey's post-test).

(E and F) Treatment of cortical neurons with translation inhibitors anisomycin (E) and cyclo-heximide (CHX) (F) severely impair neurite outgrowth but do not fully block FC-A-dependent outgrowth (n = 3, *p < 0.05, **p < 0.01, two-way ANOVA Bonferroni's post-test).

(G) Western blot of FC-A treated cortical neurons with FC-A has no effect on eIF2α phosphorylation.

(H) Densitometry of phospho eIF2α normalized to total eIF2α (n = 5). Data are presented as mean + SEM.

(I) Model of FC-A stabilization of 14-3-3 PPIs and stimulation of axon growth. Increase in 14-3-3 S58 phosphorylation during development contributes to a decline in intrinsic growth capacity. FC-A stimulates intrinsic growth capacity through downregulation of GCN1 and stabilization of 14-3-3:client protein complexes.
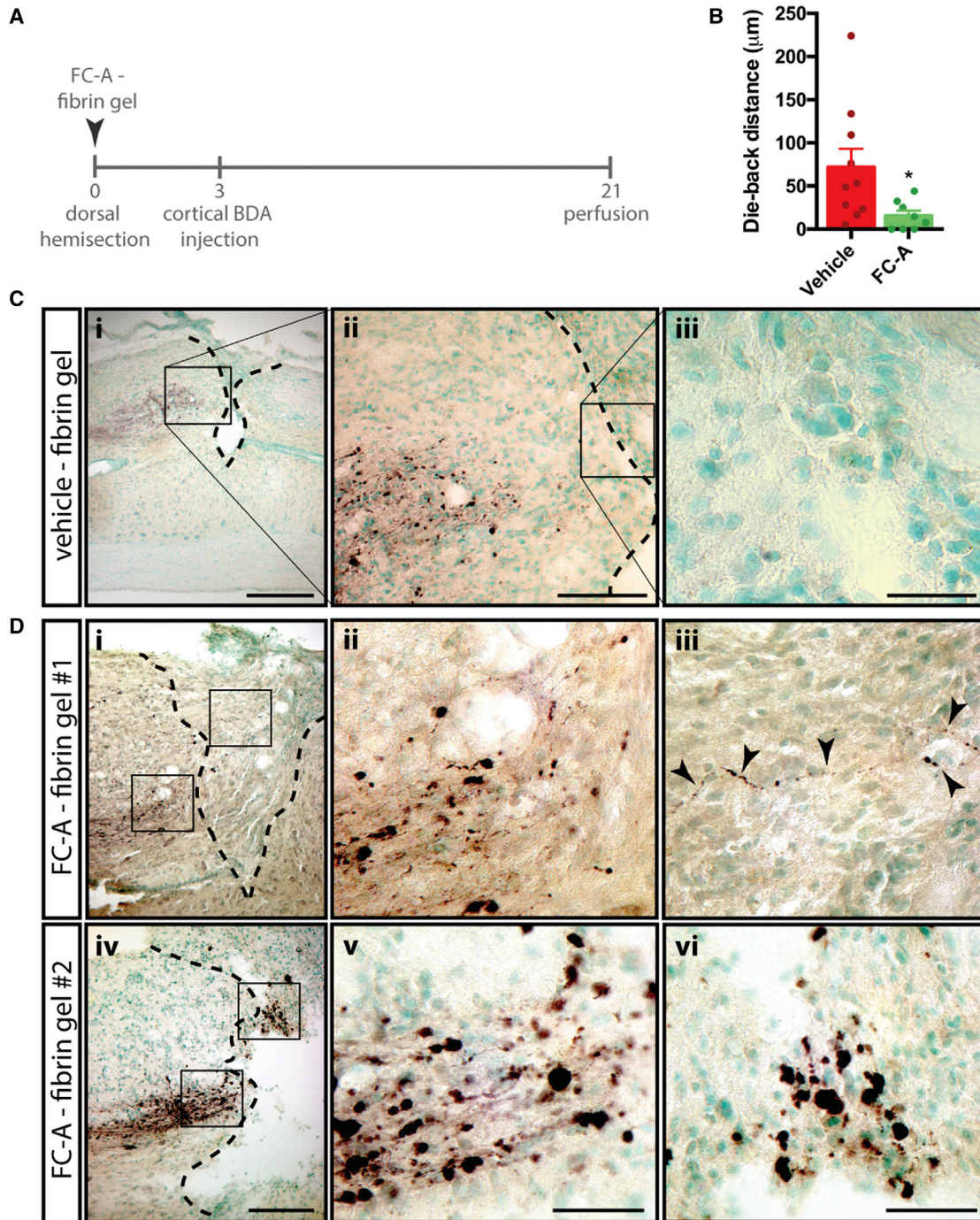
Figure 7. A Single Application of FC-A in a Fibrin Gel Reduces Corticospinal Axon Die-Back after Dorsal Hemisection Spinal Cord Injury

(A) Experimental timeline.

(B) FC-A reduces average axon die-back distance (n = 10 control, 8 FC-A-treated mice, *p < 0.05, unpaired t test). Data are presented as mean + SEM.

(C) Longitudinal section from a control vehicle-treated mouse spinal cord showing BDA-labeled corticospinal axons stopping proximal to the lesion (dotted line). Boxed area in (i) is shown at higher magnification in (ii), and boxed area in (ii) is shown at higher magnification in (iii) (scale bar i = 400 μm, ii = 100 μm, iii = 50 μm).

(D) Two FC-A-treated mice with axons and end bulbs within lesion or in close proximity to lesion border (dotted line). Boxed areas in (i) and (iv) are shown at higher magnification in (ii), (iii), (v), and (vi). Note BDA-labeled axons that extend into the lesion (one is indicated by arrowheads in iii, scale bar i and iv = 200 μm, ii, iii, v, and vi = 50 μm).
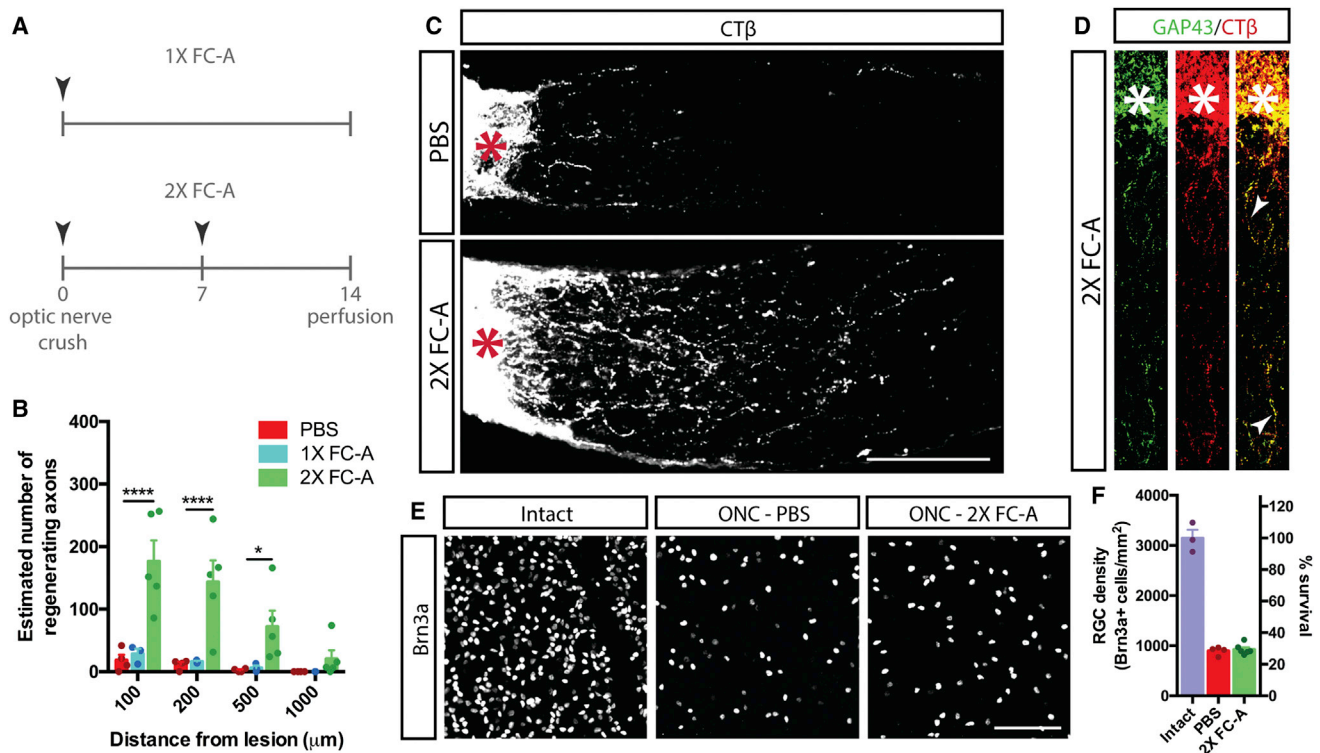
Figure 8. FC-A Stimulates Optic Nerve Regeneration

(A) Experimental timeline of optic nerve injury study.

(B) Counts of GAP43+ regenerating axons (n = 4 PBS control, 3 1× FC-A-treated, and 5 2× FC-A-treated mice, *p < 0.05, ****p < 0.0001, two-way ANOVA, Dunnett's post-test, scale bar = 100 μm).

(C) Intravitreal injections of FC-A stimulate optic nerve regeneration (lesion site marked with asterisk, scale bar = 100 μm).

(D) GAP43 and CTB staining show double labeling of regenerating axons (lesion site marked with asterisk, arrowheads indicate double-positive axons).

(E) Brn3a staining shows loss of retinal ganglion cells after ONC in retinal flat mounts (scale bar = 100 μm).

(F) Quantification of retinal ganglion cell survival (n = 3 intact, n = 4 PBS control and 6 2× FC-A-treated mice). Data are presented as mean + SEM.

end-bulbs of FC-A-treated mice were within the lesion or in close proximity to the lesion (Figures 7B and 7C). These results indicate that transient exposure to FC-A is sufficient to diminish the collapse and retraction of severed axons in vivo.

FC-A Stimulates Optic Nerve Regeneration

Next, we determined whether FC-A could stimulate CNS axon regeneration past the lesion with longer therapeutic exposure using the optic nerve crush (ONC) model and intravitreal injections. To visualize FC-A distribution after intravitreal injection, we generated an Alexa 488 FC-A conjugate. 488-FC-A was enriched in the retinal ganglion cell layer 1 day after injection, suggesting that it is readily taken up by retinal ganglion cells (RGCs) (Figure S7A). We also examined retinal GCN1 expression by western blot as a readout for activity. GCN1 was unchanged at 1 day post-injection, but significantly downregulated 3 days post-injection. Intriguingly, GCN1 levels remained suppressed 7 days post-injection, suggesting a sustained effect (Figures S7B and S7C). We next determined whether FC-A could induce axon regeneration after ONC. Mice received either 1 or 2 intravitreal injections of FC-A (Figure 8A). Cholera toxin β (CTβ) was used to trace RGC axons and GAP43 staining was used to visualize and quantify actively growing fibers. Surgeries and analysis

were performed blinded to the experimental condition. Treatment with a single injection of FC-A was insufficient to stimulate axon regeneration; however, a second injection on day 7 resulted in significant regeneration at 100, 200, and 500 μm from the lesion compared to control animals (Figures 8B and 8C). Nearly all CTβ+ axons were also GAP43+, indicating that the axons were in a growth state (Figure 8D). We also assessed RGC density in the retina using Brn3a as a marker. As expected, ONC caused a massive loss of RGCs (~70% loss of RGCs). Interestingly, FC-A-did not improve RGC survival, indicating that FC-A stimulates axon regeneration independent of cell survival (Figures 8E and 8F). These findings show that therapeutic administration of FC-A can stimulate axon regeneration after CNS injury and open the door to a new class of small molecules that could be further optimized to repair CNS damage.

DISCUSSION

We have found that 14-3-3 adaptor proteins facilitate neurite outgrowth and that 14-3-3 function is dynamically modulated by phosphorylation. Antagonism of 14-3-3 function by phosphorylation increases during development of the cortex, suggesting that this may dampen the intrinsic growth capacity of

neurons. The similar effects we observed on neurite outgrowth by manipulating the expression of 14-3-3 β, γ, or ζ suggest functional redundancy. Moreover, because manipulating the expression of single isoforms was sufficient to elicit effects on neurite outgrowth, we speculate that there is a limited pool of 14-3-3 proteins that are competent to bind to clients and that there is an excess of clients available for 14-3-3 binding. Small changes in 14-3-3 abundance could therefore have major impacts on cell signaling. While a neuroprotective role for 14-3-3s has been reported in nervous system injury models (Shimada et al., 2013; Yacoubian et al., 2010; Zhu et al., 2014), these results suggest that the promotion of 14-3-3 expression or activity may also enhance repair of damaged axons.

We have discovered that pharmacological stabilization of 14-3-3 PPIs with FC-A stimulates axon regeneration. A single treatment of the injured spinal cord prevents corticospinal fiber die-back, a mild but encouraging result that serves as proof of concept that even a brief exposure to FC-A after injury can provide benefit. We then show that more sustained dosing with FC-A is sufficient to induce axon regeneration past the lesion using the optic nerve crush model. Although modest, it is important to note that the effect on optic nerve regeneration is independent of RGC survival. A recent interesting study reported a benefit of similar magnitude with genetic overexpression of Armcx1, a regulator of mitochondrial motility, and this was accompanied by enhanced RGC survival (Cartoni et al., 2016). Moreover, extensive long-distance axon regeneration elicited by PTEN loss or overexpression of oncogenes is also accompanied by enhanced RGC survival (Belin et al., 2015; Sun et al., 2011). Our results suggest that manipulation of 14-3-3 PPIs combined with neuroprotective drugs could maximize axon regeneration. FC-A is a member of the fusicoccanes, a family of small molecules produced by plants and fungi. Cotylenin A, another member of this family, as well as semi-synthetic FC-A derivatives also act on 14-3-3 protein complexes (Anders et al., 2013; de Boer and de Vries-van Leeuwen, 2012). This new activity of FC-A may motivate the exploration of other fusicoccanes and derivatives for axon regeneration activity and the subsequent optimization of these small molecules.

We have identified GCN1 as an important target for FC-A-induced neurite outgrowth. Our results suggest that FC-A "glues" 14-3-3 to GCN1, mediating its degradation by the proteasome. It is also possible that FC-A-induced 14-3-3 binding to GCN1 impairs its interactions with other binding partners. The role of the interaction between 14-3-3 and GCN1 under baseline physiological conditions remains unknown. We found that GCN1 loss of function promotes neurite outgrowth, suggesting that it is an intrinsic inhibitor of neurite extension. GCN1 is solely known for its involvement in nutrient sensing and regulation of translation in response to stress by activating the eIF2α kinase GCN2 (Sattlegger and Hinnebusch, 2000). It is interesting to speculate that GCN1 could also be engaged by injury-induced stress and that stress response pathways could be targeted to promote axon regeneration. It is also possible that GCN1 has an important function in axon outgrowth and guidance during nervous system development, but this remains to be explored. Interestingly, it has been shown that knockdown of GCN2 enhances spontaneous neuritogenesis

and that cultured neurons from GCN2 knockout mice have enhanced neurite outgrowth. Moreover, IMPACT, a protein that binds to GCN1 and antagonizes its interaction with GCN2, promotes neurite outgrowth (Roffé et al., 2013). However, the mechanisms by which these pathways regulate neurite outgrowth are unknown. Our results suggest that protein synthesis may not be required for FC-A-induced neurite outgrowth as both CHX and anisomycin failed to fully block neurite outgrowth induction. There are no known functions of GCN1 or GCN2 outside of the eIF2 pathway. Intriguingly, GCN1 harbors a series of HEAT repeats that span the length of the protein. HEAT repeats are domains that are thought to serve as a surface for PPIs and scaffolding (Neuwald and Hirano, 2000). It is also possible that GCN1-dependent activation of GCN2 leads to the phosphorylation of other substrates involved in axon growth and regeneration.

The full repertoire of 14-3-3 PPIs that are stabilized by FC-A has yet to be defined. Because FC-A persisted in stimulating neurite outgrowth from GCN1 knockdown neurons at a high 100 μM concentration, it is likely that FC-A targets other 14-3-3:client complexes. Given the additional client proteins for which FC-A has been shown to stabilize 14-3-3 binding, we speculate that FC-A alters the 14-3-3 PPI network and has effects on multiple clients. FC-A selectively binds to both C-terminal and internal 14-3-3:client interfaces that create a compatible pocket, dependent on client protein motifs (Stevers et al., 2016). Importantly, further selectivity for specific motifs can be achieved by chemically modifying the FC-A scaffold. For instance, a semisynthetic derivative of FC-A with a fused tetrahydrofuran ring (FC-THF) has been devised to be selective for 14-3-3:client complexes that form an empty pocket in the binding groove when 14-3-3 binds to the C terminus of client proteins (Anders et al., 2013). The ability of such modifications to attain specificity for 14-3-3:client complexes raises the exciting possibility of designing compounds that can target specific 14-3-3 PPIs. Further discovery and optimization of compounds to target these interactions could result in the development of new tools to study 14-3-3s and new leads for drug development.

STAR★METHODS

Detailed methods are provided in the online version of this paper and include the following:

- KEY RESOURCES TABLE
- CONTACT FOR REAGENT AND RESOURCE SHARING
- EXPERIMENTAL MODEL AND SUBJECT DETAILS
  - Primary rodent neuron cultures
  - Human fetal neuron culture
  - Animals
- METHOD DETAILS
  - Lentiviral production and infection
  - Immunoblotting
  - Neurite outgrowth assays
  - Scratch assays
  - Fusicoccin-A conjugates
  - Affinity chromatography with Fusicoccin-A
  - Mass spectrometry analysis

- ○ Mass Spectrometry data analysis
- ○ Co-immunoprecipitation
- ○ Dorsal hemisection spinal cord injuries
- ○ Optic nerve crush
- ○ Regeneration and survival quantification
- ● QUANTIFICATION AND STATISTICAL ANALYSIS

REFERENCES

Anders, C., Higuchi, Y., Koschinsky, K., Bartel, M., Schumacher, B., Thiel, P., Nitta, H., Preisig-Müller, R., Schlichthörl, G., Renigunta, V., et al. (2013). A semisynthetic fusicoccane stabilizes a protein-protein interaction and enhances the expression of K+ channels at the cell surface. Chem. Biol. *20*, 583–593.

Belin, S., Nawabi, H., Wang, C., Tang, S., Latremoliere, A., Warren, P., Schorle, H., Uncu, C., Woolf, C.J., He, Z., and Steen, J.A. (2015). Injury-induced decline of intrinsic regenerative ability revealed by quantitative proteomics. Neuron *86*, 1000–1014.

Bury, M., Andolfi, A., Rogister, B., Cimmino, A., Mégalizzi, V., Mathieu, V., Feron, O., Evidente, A., and Kiss, R. (2013). Fusicoccin a, a phytotoxic carbotricyclic diterpene glucoside of fungal origin, reduces proliferation and invasion of glioblastoma cells by targeting multiple tyrosine kinases. Transl. Oncol. *6*, 112–123.

Camoni, L., Di Lucente, C., Visconti, S., and Aducci, P. (2011). The phytotoxin fusicoccin promotes platelet aggregation via 14-3-3-glycoprotein Ib-IX-V interaction. Biochem. J. *436*, 429–436.

Cartoni, R., Norsworthy, M.W., Bei, F., Wang, C., Li, S., Zhang, Y., Gabel, C.V., Schwarz, T.L., and He, Z. (2016). The mammalian-specific protein armcx1 regulates mitochondrial transport during axon regeneration. Neuron *92*, 1294–1307.

Chandran, V., Coppola, G., Nawabi, H., Omura, T., Versano, R., Huebner, E.A., Zhang, A., Costigan, M., Yekkirala, A., Barrett, L., et al. (2016). A systems-level analysis of the peripheral nerve intrinsic axonal growth program. Neuron *89*, 956–970.

Cheah, P.S., Ramshaw, H.S., Thomas, P.Q., Toyo-Oka, K., Xu, X., Martin, S., Coyle, P., Guthridge, M.A., Stomski, F., van den Buuse, M., et al. (2012). Neurodevelopmental and neuropsychiatric behaviour defects arise from 14-3-3ζ deficiency. Mol. Psychiatry *17*, 451–466.

Choi, H., Larsen, B., Lin, Z.Y., Breitkreutz, A., Mellacheruvu, D., Fermin, D., Qin, Z.S., Tyers, M., Gingras, A.C., and Nesvizhskii, A.I. (2011). SAINT: probabilistic scoring of affinity purification-mass spectrometry data. Nat. Methods *8*, 70–73.

Corradi, V., Mancini, M., Manetti, F., Petta, S., Santucci, M.A., and Botta, M. (2010). Identification of the first non-peptidic small molecule inhibitor of the c-Abl/14-3-3 protein-protein interactions able to drive sensitive and Imatinib-resistant leukemia cells to apoptosis. Bioorg. Med. Chem. Lett. *20*, 6133–6137.

de Boer, A.H., and de Vries-van Leeuwen, I.J. (2012). Fusicoccanes: diterpenes with surprising biological functions. Trends Plant Sci. *17*, 360–368.

De Vries-van Leeuwen, I.J., da Costa Pereira, D., Flach, K.D., Piersma, S.R., Haase, C., Bier, D., Yalcin, Z., Michalides, R., Feenstra, K.A., Jiménez, C.R., et al. (2013). Interaction of 14-3-3 proteins with the estrogen receptor alpha F domain provides a drug target interface. Proc. Natl. Acad. Sci. USA *110*, 8894–8899.

Feyerabend, M., and Weiler, E.W. (1987). Monoclonal antibodies against fusicoccin with binding characteristics similar to the putative fusicoccin receptor of higher plants. Plant Physiol. *85*, 835–840.

Gómez-Suárez, M., Gutiérrez-Martínez, I.Z., Hernández-Trejo, J.A., Hernández-Ruiz, M., Suárez-Pérez, D., Candelario, A., Kamekura, R., Medina-Contreras, O., Schnoor, M., Ortiz-Navarrete, V., et al. (2016). 14-3-3 Proteins regulate Akt Thr308 phosphorylation in intestinal epithelial cells. Cell Death Differ. *23*, 1060–1072.

Gu, Y.M., Jin, Y.H., Choi, J.K., Baek, K.H., Yeo, C.Y., and Lee, K.Y. (2006). Protein kinase A phosphorylates and regulates dimerization of 14-3-3 epsilon. FEBS Lett. *580*, 305–310.

Huebner, E.A., Kim, B.G., Duffy, P.J., Brown, R.H., and Strittmatter, S.M. (2011). A multi-domain fragment of Nogo-A protein is a potent inhibitor of cortical axon regeneration via Nogo receptor 1. J. Biol. Chem. *286*, 18026–18036.

Kent, C.B., Shimada, T., Ferraro, G.B., Ritter, B., Yam, P.T., McPherson, P.S., Charron, F., Kennedy, T.E., and Fournier, A.E. (2010). 14-3-3 proteins regulate protein kinase a activity to modulate growth cone turning responses. J. Neurosci. *30*, 14059–14067.

Liu, K., Lu, Y., Lee, J.K., Samara, R., Willenberg, R., Sears-Kraxberger, I., Tedeschi, A., Park, K.K., Jin, D., Cai, B., et al. (2010). PTEN deletion enhances the regenerative ability of adult corticospinal neurons. Nat. Neurosci. *13*, 1075–1081.

Masters, S.C., and Fu, H. (2001). 14-3-3 proteins mediate an essential anti-apoptotic signal. J. Biol. Chem. *276*, 45193–45200.

Mohammad, D.K., Nore, B.F., Hussain, A., Gustafsson, M.O., Mohamed, A.J., and Smith, C.I. (2013). Dual phosphorylation of Btk by Akt/protein kinase b provides docking for 14-3-3ζ, regulates shuttling, and attenuates both tonic and induced signaling in B cells. Mol. Cell. Biol. *33*, 3214–3226.

Morquette, B., Morquette, P., Agostinone, J., Feinstein, E., McKinney, R.A., Kolta, A., and Di Polo, A. (2015). REDD2-mediated inhibition of mTOR promotes dendrite retraction induced by axonal injury. Cell Death Differ. *22*, 612–625.

Neuwald, A.F., and Hirano, T. (2000). HEAT repeats associated with condensins, cohesins, and other complexes involved in chromosome-related functions. Genome Res. *10*, 1445–1452.

O'Donovan, K.J., Ma, K., Guo, H., Wang, C., Sun, F., Han, S.B., Kim, H., Wong, J.K., Charron, J., Zou, H., et al. (2014). B-RAF kinase drives developmental axon growth and promotes axon regeneration in the injured mature CNS. J. Exp. Med. *211*, 801–814.

Park, K.K., Liu, K., Hu, Y., Smith, P.D., Wang, C., Cai, B., Xu, B., Connolly, L., Kramvis, I., Sahin, M., and He, Z. (2008). Promoting axon regeneration in the adult CNS by modulation of the PTEN/mTOR pathway. Science *322*, 963–966.

Powell, D.W., Rane, M.J., Joughin, B.A., Kalmukova, R., Hong, J.H., Tidor, B., Dean, W.L., Pierce, W.M., Klein, J.B., Yaffe, M.B., and McLeish, K.R. (2003). Proteomic identification of 14-3-3zeta as a mitogen-activated protein kinase-activated protein kinase 2 substrate: role in dimer formation and ligand binding. Mol. Cell. Biol. *23*, 5376–5387.

Qureshi, H.Y., Han, D., MacDonald, R., and Paudel, H.K. (2013). Overexpression of 14-3-3z promotes tau phosphorylation at Ser262 and accelerates proteosomal degradation of synaptophysin in rat primary hippocampal neurons. PLoS ONE *8*, e84615.

Roffé, M., Hajj, G.N., Azevedo, H.F., Alves, V.S., and Castilho, B.A. (2013). IMPACT is a developmentally regulated protein in neurons that opposes the eukaryotic initiation factor 2α kinase GCN2 in the modulation of neurite outgrowth. J. Biol. Chem. *288*, 10860–10869.

Sattlegger, E., and Hinnebusch, A.G. (2000). Separate domains in GCN1 for binding protein kinase GCN2 and ribosomes are required for GCN2 activation in amino acid-starved cells. EMBO J. *19*, 6622–6633.

Shen, Y.H., Godlewski, J., Bronisz, A., Zhu, J., Comb, M.J., Avruch, J., and Tzivion, G. (2003). Significance of 14-3-3 self-dimerization for phosphorylation-dependent target binding. Mol. Biol. Cell *14*, 4721–4733.

Shimada, T., Fournier, A.E., and Yamagata, K. (2013). Neuroprotective function of 14-3-3 proteins in neurodegeneration. BioMed Res. Int. *2013*, 564534.

Stevers, L.M., Lam, C.V., Leysen, S.F.R., Meijer, F.A., van Scheppingen, D.S., de Vries, R.M.J.M., Carlile, G.W., Milroy, L.G., Thomas, D.Y., Brunsveld, L., et al. (2016). Characterization and small-molecule stabilization of the multisite tandem binding between 14-3-3 and the R domain of CFTR. Proc. Natl. Acad. Sci. USA *113*, E1152–E1161.

Sun, F., Park, K.K., Belin, S., Wang, D., Lu, T., Chen, G., Zhang, K., Yeung, C., Feng, G., Yankner, B.A., and He, Z. (2011). Sustained axon regeneration induced by co-deletion of PTEN and SOCS3. Nature *480*, 372–375.

Toyo-oka, K., Shionoya, A., Gambello, M.J., Cardoso, C., Leventer, R., Ward, H.L., Ayala, R., Tsai, L.H., Dobyns, W., Ledbetter, D., et al. (2003). 14-3-3epsilon is important for neuronal migration by binding to NUDEL: a molecular explanation for Miller-Dieker syndrome. Nat. Genet. *34*, 274–285.

Toyo-oka, K., Wachi, T., Hunt, R.F., Baraban, S.C., Taya, S., Ramshaw, H., Kaibuchi, K., Schwarz, Q.P., Lopez, A.F., and Wynshaw-Boris, A. (2014). 14-3-3ε and ζ regulate neurogenesis and differentiation of neuronal progenitor cells in the developing brain. J. Neurosci. *34*, 12168–12181.

Tzivion, G., Shen, Y.H., and Zhu, J. (2001). 14-3-3 proteins; bringing new definitions to scaffolding. Oncogene *20*, 6331–6338.

Wang, B., Liu, K., Lin, H.Y., Bellam, N., Ling, S., and Lin, W.C. (2010). 14-3-3Tau regulates ubiquitin-independent proteasomal degradation of p21, a novel mechanism of p21 downregulation in breast cancer. Mol. Cell. Biol. *30*, 1508–1527.

Woodcock, J.M., Murphy, J., Stomski, F.C., Berndt, M.C., and Lopez, A.F. (2003). The dimeric versus monomeric status of 14-3-3zeta is controlled by phosphorylation of Ser58 at the dimer interface. J. Biol. Chem. *278*, 36323–36327.

Würtele, M., Jelich-Ottmann, C., Wittinghofer, A., and Oecking, C. (2003). Structural view of a fungal toxin acting on a 14-3-3 regulatory complex. EMBO J. *22*, 987–994.

Yacoubian, T.A., Slone, S.R., Harrington, A.J., Hamamichi, S., Schieltz, J.M., Caldwell, K.A., Caldwell, G.A., and Standaert, D.G. (2010). Differential neuroprotective effects of 14-3-3 proteins in models of Parkinson's disease. Cell Death Dis. *1*, e2.

Yam, P.T., Kent, C.B., Morin, S., Farmer, W.T., Alchini, R., Lepelletier, L., Colman, D.R., Tessier-Lavigne, M., Fournier, A.E., and Charron, F. (2012). 14-3-3 proteins regulate a cell-intrinsic switch from sonic hedgehog-mediated commissural axon attraction to repulsion after midline crossing. Neuron *76*, 735–749.

Yin, Y., Cui, Q., Li, Y., Irwin, N., Fischer, D., Harvey, A.R., and Benowitz, L.I. (2003). Macrophage-derived factors stimulate optic nerve regeneration. J. Neurosci. *23*, 2284–2293.

Zhou, J., Shao, Z., Kerkela, R., Ichijo, H., Muslin, A.J., Pombo, C., and Force, T. (2009). Serine 58 of 14-3-3zeta is a molecular switch regulating ASK1 and oxidant stress-induced cell death. Mol. Cell. Biol. *29*, 4167–4176.

Zhu, Y., Bu, Q., Liu, X., Hu, W., and Wang, Y. (2014). Neuroprotective effect of TAT-14-3-3ε fusion protein against cerebral ischemia/reperfusion injury in rats. PLoS ONE *9*, e93334.

STAR★METHODS

KEY RESOURCES TABLE

REAGENT or RESOURCE	SOURCE	IDENTIFIER
Antibodies		
anti-pan-14-3-3	Santa Cruz	Cat#sc-1657; RRID: AB_626618
anti-pan-14-3-3-HRP	Santa Cruz	Cat#sc-1657 HRP; RRID: AB_626618
anti-14-3-3β	Santa Cruz	Cat#sc-25276; RRID: AB_626617
anti-14-3-3γ	Santa Cruz	Cat#sc-731; RRID: AB_2217962
anti-14-3-3ζ	Santa Cruz	Cat#sc-1019; RRID: AB_2218378
anti-14-3-3ζ phospho-S58	Abcam	Cat#ab51109; RRID: AB_867443
anti-myc (clone 9E10)	Sigma	Cat#M4439; RRID: AB_439694
anti-GCN1L1	Abcam	Cat#ab86139; RRID: AB_1925025
anti-Brn3a	Santa Cruz	Cat#sc-31984; RRID: AB_2167511
anti-GAP43	Novus	Cat#NBP1-41123; RRID: AB_10005026
Anti-Tau-1 (clone PC1C6)	Millipore	Cat#IHCR1015-6; RRID: AB_2139842
Anti-betaIII tubulin (clone Tuj1)	BioLegend	Cat# 801201 or 801202; RRID: AB_2313773 or RRID: AB_10063408
Alexa 488 anti-mouse	Thermo Fisher	Cat#A11029; RRID: AB_138404
Alexa 568 anti-mouse	Thermo Fisher	Cat#A11031; RRID: AB_144696
Alexa 647 anti-mouse	Thermo Fisher	Cat#A21235; RRID: AB_141693
Alexa 488 anti-rabbit	Thermo Fisher	Cat#A11034; RRID: AB_2576217
Alexa 568 anti-rabbit	Thermo Fisher	Cat#A11011; RRID: AB_143157
Alexa 647 anti-rabbit	Thermo Fisher	Cat#A21244; RRID: AB_141663
Alexa 568 anti-goat	Thermo Fisher	Cat#A11057; RRID: AB_14258
Alexa 488 anti-sheep	Thermo Fisher	Cat#A11015; RRID: AB_141362
Anti-mouse HRP	Jackson ImmunoResearch	Cat#115-035-071; RRID: AB_2338506
Anti-Rabbit HRP	Jackson ImmunoResearch	Cat#111-035-046; RRID: AB_2337939
Bacterial and Virus Strains		
3rd generation lentiviral system	Kent et al., 2010	N/A
Biological Samples		
Human fetal brain tissue	Human Fetal Tissue Repository (Albert Einstein College)	N/A
Chemicals, Peptides, and Recombinant Proteins		
Fusicoccin-A	Santa Cruz or Enzo	Cat#BML-EI334 or Cat#sc-200754
BV02 (14-3-3 antagonist II)	Millipore	Cat#100082
Y27632	Millipore	Cat#688001
R18 peptide	Enzo	Cat#BML-P214
Alexa 594 Cholera toxin beta	Thermo Fisher	Cat#C22842
SiMAG-hydrazide beads	Chemicell	N/A
Aggrecan	Sigma	Cat#A1960
KT5720	Sigma	Cat#K3761
Rapamycin	Sigma	Cat#R0395
Alexa 568 phalloidin	Thermo Fisher	Cat# A12380
Biotinylated dextran amine (10kDa MW)	Molecular probes	Cat#D-1956
DAB tablets	Sigma	Cat#D-5905
ABC Kit	Vector Laboratories	Cat#PK-6100
Alexa 488 hydrazide	Thermo Fisher	Cat#A10436

(Continued on next page)

Continued

REAGENT or RESOURCE	SOURCE	IDENTIFIER
Critical Commercial Assays		
Evicel Fibrin Sealant Kit	Ethicon	Cat#3901
In situ cell death detection kit TMR red	Roche	Cat#12156792910
Experimental Models: Cell Lines		
Primary cortical neurons – E18/19 Sprague Dawley rat	Charles River Labs	N/A
Primary cortical neurons – E16/17 CD-1 mouse	Charles River Labs	N/A
Experimental Models: Organisms/Strains		
C57BL/6 mice	Charles River Labs	N/A
Recombinant DNA		
pRRLsinPPT- 14-3-3β shRNA	Kent et al., 2010	N/A
pRRLsinPPT- 14-3-3γ shRNA	Kent et al., 2010	N/A
pRRLsinPPT- 14-3-3ζ shRNA	Kent et al., 2010	N/A
pRRLsinPPT- myc-14-3-3β	Kent et al., 2010	N/A
pRRLsinPPT- myc-14-3-3γ	Kent et al., 2010	N/A
pRRLsinPPT- myc-14-3-3ζ	Kent et al., 2010	N/A
pMDLg	Kent et al., 2010	N/A
pMD2g	Kent et al., 2010	N/A
pRSV-Rev	Kent et al., 2010	N/A
pCS4- WT 14-3-3ζ	Gu et al., 2006	N/A
pCS4- 14-3-3ζ S58A	Gu et al., 2006	N/A
pCS4- 14-3-3ζ S58E	Gu et al., 2006	N/A
pEYFP-C1-Difopein	Masters and Fu, 2001	N/A
pLKO- GCN1 shRNA	Sigma MISSION library	Cat#TRCN0000251695
pRRL-EGFP	Kent et al., 2010	N/A
Software and Algorithms		
MetaXpress – Automated Neurite Outgrowth Module	Molecular Devices	N/A
Prism 6	GraphPad	RRID: SCR_002798
ImageJ	NIH	RRID: SCR_003070
Other		
ImageXpress – Automated High Content Imaging System	Molecular Devices	N/A
Nucleofector	Lonza	AAB-1001

CONTACT FOR REAGENT AND RESOURCE SHARING

Further information and requests for resources and reagents should be directed to and will be fulfilled by the Lead Contact, Dr. Alyson Fournier (alyson.fournier@mcgill.ca).

EXPERIMENTAL MODEL AND SUBJECT DETAILS

Primary rodent neuron cultures

All studies were approved by the McGill University Animal Care and Use Committee. For cortical neuron cultures, cortices from male and female embryos were dissected from E18-19 Sprague Dawley rat or E16-17 CD-1 mouse in cold Leibovitz L15 medium (Thermo Fisher). Isolated cortices were incubated in 0.25% trypsin-EDTA and dissociated into a single cell suspension by gentle trituration. Neurons were seeded onto culture dishes coated with 100 μg/mL poly-l-lysine (PLL). For reseeding of neurons onto aggrecan substrate, triplicate wells in a 96-well plate were coated with 0.5, 1 or 2 μg aggrecan for 2 hr at 37°C. Culture medium consisted of Neurobasal medium supplemented with 2% B27, 1% N2, 1% penicillin/streptomycin and 2mM L-glutamine.

Human fetal neuron culture

Human fetal brain tissue (male and female, 16–18 gestational weeks) was acquired from the Human Fetal Tissue Repository (Albert Einstein College of Medicine, Bronx, NY). Tissue was dissociated in 0.25% trypsin-EDTA and 25 μg/mL DNase and then passed through a 140 μm nylon mesh. Neurons were seeded onto culture dishes coated with 100 μg/mL PLL. Culture medium consisted of Neurobasal medium supplemented with 2% B27, 1% N2, 1% penicillin/streptomycin and 2 mM L-glutamine.

Animals

Adult female C57BL/6 mice (8-10 weeks of age) were used for spinal cord injury studies. Age and sex matched C57BL/6 mice (male and female, 8-14 weeks of age) were used for optic nerve crush studies. Experimental conditions were randomized and surgeries were performed blinded to the experimental condition.

METHOD DETAILS

Lentiviral production and infection

Lentiviruses were produced in HEK293T cells using a 3rd generation system. HEK293T were grown in DMEM 10% fetal bovine serum to ∼80% confluence in 15cm plates and transfected (Lipofectamine 2000) with pRRL 14-3-3 shRNA or 14-3-3-myc plasmid (27 μg) along with packaging plasmids, pMD2g (8 μg), pMDLg (13 μg) and pRSV-Rev (6.5 μg) and viral supernatants were collected over a period of 2 days. Purified virus was isolated by overnight centrifugation at 7500 g and subsequently titered in HEK293T cells. Rat cortical neurons were infected overnight with purified lentiviruses at a multiplicity of infection (MOI) of 5 for knockdown or 2-3 for over-expression of 14-3-3 isoforms. The following day, the medium was replaced and half was replenished every 3-4 days thereafter.

Immunoblotting

Cortical neurons were lysed in ice cold lysis buffer composed of 100 mM NaCl, 50 mM Tris-HCl, 5 mM EDTA, 2 mM MgCl$_2$, 10% glycerol and 1% NP-40 supplemented with protease inhibitors (Complete protease inhibitor cocktail, Roche) and phosphatase inhibitors (10 mM sodium fluoride and 1 mM sodium orthovanadate). For retinal and cortex lysates, retinae or cortices were collected, flash frozen in liquid nitrogen and subsequently pulverized in complete lysis buffer. Lysates were clarified by centrifugation and protein concentration was determined by DC protein assay (Bio-Rad). Lysates were boiled in sample buffer, separated by SDS-PAGE and transferred to PVDF membranes. Membranes were blocked with 5% milk TBS-T for 1 hr, probed with primary antibody for 1 hr at room temperature or overnight at 4°C and probed with HRP-conjugated secondary antibodies for 1 hr at room temperature. The following primary antibodies were used: anti-pan-14-3-3 (1:5000, RRID: AB_626618), anti-pan-14-3-3-HRP (1:5000, RRID: AB_626618), anti-14-3-3β (1:5000, RRID: AB_626617), anti-14-3-3γ (1:2000, RRID: AB_2217962), anti-14-3-3ζ (1:5000, RRID: AB_2218378), anti-14-3-3ζ phospho-S58 (1:2000, RRID: AB_867443), anti-myc clone 9E10 (1:1000, RRID: AB_439694), anti-GCN1L1 (1:500, RRID: AB_1925025). HRP-conjugated secondary antibodies were from Jackson ImmunoResearch.

Neurite outgrowth assays

Cortical neurons were seeded in 96-well plates at 7,000 cells per well. After 2hr, medium was replaced with fresh culture medium containing vehicle or indicated doses of FC-A, Y27632, BV02, KT5720, or Rapamycin. On day 1 of culture (DIV1) the neurons were fixed with 4% paraformaldehyde/20% sucrose, permeabilized with 0.2% Triton-X, blocked with 5% BSA, and stained with anti-βIII tubulin (1:1000, RRID: AB_2313773 or AB_10063408), Hoechst 33342 (1:10000) and fluorescent secondary antibodies (1:1000). Apoptotic cells were identified by TUNEL staining (in situ cell death detection kit TMR red, Roche #12156792910). For human fetal neurite outgrowth, cultures were treated with FC-A on DIV2 and fixed and stained on DIV4. For re-seeding of neurons infected with lentiviruses, neurons in 6-well plates were incubated with 0.125% trypsin in Neurobasal medium for 10min at 37°C, gently triturated, replated in 96-well plates at 7,000 cells per well, treated with vehicle or 25 μM FC-A and grown for an additional 3 days before fixing and staining. For overexpression of WT, S58A and S58E 14-3-3ζ (kindly provided by Dr. Kwang Youl Lee, (Gu et al., 2006)) dissociated rat cortical neurons were electroporated with a 2 μg:1 μg mixture of 14-3-3 plasmid and a plasmid encoding EGFP and fixed and stained on DIV2; for knockdown of GCN1, mouse cortical neurons were electroporated with a 2 μg:1 μg mixture of GCN1 shRNA plasmid and a plasmid encoding EGFP and fixed and stained on DIV3; for overexpression of difopein-YFP (kindly provided by Dr. Haian Fu, (Masters and Fu, 2001)) cortical neurons were electroporated with 2 μg difopein-YFP or a plasmid encoding GFP; for rescue of 14-3-3 knockdowns, cortical neurons were electroporated with a 1 μg:2 μg mixture of pRRL 14-3-3 shRNA and RNAi resistant pRRL 14-3-3-myc. Electroporations were performed using the Nucleofector kit, Lonza, program O-003 for rat or O-005 for mouse neurons in Mirus electroporation solution (MIR50111). Automated image acquisition and analysis were performed using an ImageXpress system and the neurite outgrowth module of the MetaXpress software (Molecular Devices). All assays were performed with 3-12 replicates per condition from 3-6 independent experiments.

Scratch assays

Rat cortical neurons were seeded in 96-well plates at 30,000 cells per well, half the medium was replenished every 3-4 days and on DIV10, a scratch was made across the center of each well with a plastic P10 pipet tip. Immediately after scratching, compounds were added to the wells. The following day, the cultures were fixed with 4% paraformaldehyde/20% sucrose, permeabilized with

0.2% Triton-X, blocked with 5% BSA, and stained with anti-βIII tubulin (1:1000) or anti-Tau-1 (1:500, RRID: AB_2139842) or anti-14-3-3ζ (1:1000), Alexa-568-phalloidin (1:1000) and fluorescent secondary antibodies (1:1000). Images of βIII tubulin stained axons were acquired in the center of each scratch and thresholded in ImageJ. The outline of each scratch was traced and the percent area of βIII tubulin stained neurites in the central ∼70% of the scratch was measured in ImageJ. All assays were performed with 6-12 replicates per condition from 3 independent experiments.

Fusicoccin-A conjugates

For conjugation of FC-A to beads, the vinylic carbon on the sugar group of FC-A was oxidized to generate an aldehyde as previously described (Feyerabend and Weiler, 1987). Briefly, FC-A dissolved in tetrahydrofuran (THF) was oxidized with OsO_4 and $NaIO_4$ to generate FC-A-aldehyde. The following day, the product was loaded onto a Sep Pak C18 cartridge (Millipore Waters) and eluted with methanol. The efficiency of FC-A-aldehyde formation was determined by thin layer chromatography and the FC-aldehyde was then incubated with magnetic SiMAG hydrazide-beads (Chemicell) to couple the FC-A-aldehyde to the beads through the formation of hydrazone bonds. Unreacted sites were blocked with glyceraldehyde. Magnetic beads coupled to glyceraldehyde were used as control beads. The same strategy was used to couple FC-A to Alexa 488-hydrazide.

Affinity chromatography with Fusicoccin-A

Rat cortical neurons were plated in 10 cm dishes and on DIV7 the neurons were lysed in ice cold lysis buffer composed of 100 mM NaCl, 50 mM Tris-HCl, 5 mM EDTA, 2 mM $MgCl_2$, 10% glycerol and 1% NP-40 supplemented with protease inhibitors (Complete protease inhibitor cocktail, Roche) and phosphatase inhibitors (10 mM sodium fluoride and 1mM sodium orthovanadate). Lysates were clarified by centrifugation and protein concentration was determined by DC protein assay (Bio-Rad). 1.5mg of lysate was added to 30 μL pre-washed control beads or FC-A-beads in 500 μL lysis buffer. Lysates were incubated with the beads and vehicle or 10 μM R18 or 100 μM FC-A for 2hr at 4°C with rotation and subsequently washed 3 times with lysis buffer and boiled in 2X SDS sample buffer for western blot analysis.

Mass spectrometry analysis

For mass spectrometry, FC-A beads were washed 5 times and resuspended in 50mM ammonium bicarbonate pH 8.5 with 1 μg of trypsin (Promega) and incubated at 37°C overnight with agitation. The next day, an additional 1 μg of trypsin was added and samples were incubated for 3 hr at 37°C. Beads were pelleted and the supernatant was transferred to a fresh tube. Beads were then rinsed two times with 100 μL of MS-grade water. All supernatants were combined and dried in a vacuum centrifuge. Tryptic peptides were resuspended in 15 μL of 5% formic acid; 5 μL were used per analysis.

An Orbitrap Fusion mass spectrometer equipped with a nanoelectrospray ion source (Thermo Scientific) and coupled to a UltiMate 3000 nanoRSLC (Dionex/Thermo) was used for peptide analyses. Mass spectra were acquired using a data dependent acquisition mode using Thermo XCalibur software version 3.0.63. Full scan mass spectra (350 to 1800 m/z) were acquired in the orbitrap using an automatic gain control target of 4e5, a maximum injection time of 50 ms and a resolution of 120 000. Selected ions were isolated using the quadrupole analyzer in a window of 1.6 m/z and fragmented by higher energy collision-induced dissociation (HCD) with 35% of collision energy. The resulting fragments were detected by the linear ion trap at a rapid scan rate. Dynamic exclusion of previously fragmented peptides was set for a period of 20 s and a tolerance of 10 ppm.

All MS/MS peak lists were generated using Thermo Proteome Discoverer version 1.4.0.288 (Thermo Scientific). MGF sample files were then analyzed using Mascot (Matrix Science, London, UK; version 2.4.0) and X! Tandem (The GPM, thegpm.org; version CYCLONE (2010.12.01.1). Both were set up to search Uniprot Rattus norvegicus database (November 2014 release, 37218 entries) assuming the digestion enzyme trypsin. They were searched with a fragment ion mass tolerance of 0.60 Da and a parent ion tolerance of 10 ppm. Carbamidomethyl of cysteine was specified as a fixed modification. Deamidated of asparagine and glutamine, oxidation of methionine and phospho of serine, threonine and tyrosine were specified as variable modifications. Two miscleavages were allowed.

Mass Spectrometry data analysis

Scaffold (version 4.0.1, Proteome Software) was used to validate MS/MS based peptide and protein identifications. Protein identifications were accepted if they could be established at greater than 99.0% probability to achieve an FDR less than 1.0% and contained at least 1 identified peptides. Protein probabilities were assigned by the Protein Prophet algorithm (PMID: 14632076). Proteins that contained similar peptides and could not be differentiated based on MS/MS analysis alone were grouped to satisfy the principles of parsimony.

MS data were analyzed with SAINTexpress, a simplified version of the Significance Analysis of INTeractome method described previously (PMID: 24513533) via the CRAPome website (PMID: 23921808). SAINT probabilities were calculated using MS data from control beads. The average probability is reported as the final SAINT score in the table. Preys with an average greater or equal to 0.9 were considered "true" interactors (Table S1).

Co-immunoprecipitation

Rat cortical neurons were lysed in ice cold lysis buffer composed of 100 mM NaCl, 50 mM Tris-HCl, 5mM EDTA, 2 mM $MgCl_2$, 10% glycerol and 0.5% NP-40 supplemented with protease and phosphatase inhibitors. 1.5mg of cell lysate was pre-cleared with protein A/G beads (Santa Cruz, sc-2003) and subsequently incubated with 1 μg of anti-GCN1L1 and vehicle or 50 μM FC-A for 2hr at 4°C with rotation. Beads were washed 3 times with lysis buffer and boiled in 2X SDS sample buffer for western blot analysis. Blots were probed with anti-GCN1L1 (1:500, RRID: AB_1925025) and anti-pan-14-3-3-HRP (1:5000).

Dorsal hemisection spinal cord injuries

Adult female C57BL/6 mice (8-10 weeks of age) were deeply anesthetized with ketamine:xylazine:acepromazine (50:5:1 mg/kg) and a laminectomy was done to expose the T9 thoracic spinal cord. Dorsal hemisection of the spinal cord was performed with spring micro-scissors to cut through the central canal. 200 μg FC-A solubilized in a 1:3 stock of ethanol:PBS was diluted in a thrombin solution into a final volume of 25 μL, quickly mixed with 25 μL of a fibrinogen solution and immediately applied directly onto the injury site, forming a viscous gel. Thrombin and fibrinogen solutions were purchased as a kit (Evicel Fibrin Sealant). Mice received 0.2 μL bilateral injections of 10% biotinylated dextran amine (BDA) into the sensorimotor cortex with a glass pipette. On day 21, mice were transcardially perfused with 4% PFA and the spinal cord was cryoprotected in 30% sucrose. 25 μm longitudinal sections were collected on slides, incubated in 0.6% hydrogen peroxide for 3hr, and overnight with streptavidin complex (Vector Laboratories). Sections were reacted with diaminobenzidine to visualize the streptavidin–biotin–dextranamine complex and counterstained with methyl green. Scar borders were determined from the methyl green stain and quantification of axonal die-back distance was assessed blinded to the experimental condition by measuring and averaging the distances between the 5 closest end-bulbs from the edge of the lesion. Animals that had incomplete lesions were excluded from the study. Sample sizes were based on previous spinal cord injury studies (Liu et al., 2010). All surgeries were randomized and performed blinded to the experimental condition in two independent cohorts.

Optic nerve crush

Age and sex matched C57BL/6 mice (male and female, 8-14 weeks of age) were anesthetized with isoflurane and an incision was made above the left orbit. Under a surgical microscope, the extra-ocular muscles were resected to expose the underlying optic nerve. The optic nerve was crushed 0.5-1 mm behind the optic nerve head with fine forceps (Dumont #5) for 10 s. Care was taken to avoid damaging the ophthalmic artery. Vascular integrity of the retina was assessed by a fundus examination. For intravitreal injections, a small puncture was made in the sclera with a 30-gauge needle and 2 μL of PBS or FC-A (1 μg/μL solution in PBS) was injected into the wound using a Hamilton syringe. The needle was held in place for ∼2 min to avoid reflux and the puncture was sealed with surgical glue. Mice that had significant reflux were excluded from the study. Injections of PBS or FC-A were performed immediately after injury and again 7 days after injury. Cholera toxin injections (1 μL) were performed on day 12-13. Mice were transcardially perfused with 4% PFA on day 14. Optic nerves and eyes were harvested on day 14 and post-fixed in 4% PFA for 2hr. Retinal flat mounts were prepared and stained with anti-Brn3a (0.3 μg/mL, RRID: AB_2167511). Optic nerves were cryoprotected in 30% sucrose at 4°C overnight and embedded in OCT. Longitudinal sections (14 μm thickness) were collected on slides, permeabilized and blocked with 0.3% Triton-X in 5% BSA for 1hr at room temperature, stained with anti-GAP43 (1:1000, RRID: AB_10005026) overnight at 4°C, washed 3 times with PBS and stained with Alexa 488-conjugated secondary antibody (1:1000). Sample sizes were based on previous optic nerve injury studies (Chandran et al., 2016). All surgeries and injections were randomized and performed blinded to the experimental condition.

Regeneration and survival quantification

The number of regenerating axons visualized by GAP43 staining were counted at distances of 100, 200, 500 and 1000 μm from the lesion. The estimated total number of regenerating axons Σa_d per nerve with a radius r, in a section with thickness t, at a distance d from the lesion was determined using the formula $\Sigma a_d = \pi r^2$ x (axons/mm width) x t, as previously described(Yin et al., 2003). Axon counts were performed blinded to the experimental condition from 3-4 sections per mouse. Mice that had GAP43+ axons near the optic chiasm reflecting spared fibers were excluded from the study. To determine the RGC density per mm^2, Brn3a+ RGCs were counted in ImageJ (Morquette et al., 2015).

QUANTIFICATION AND STATISTICAL ANALYSIS

All statistical tests were performed with GraphPad Prism 6. As indicated in figure legends, the following statistical tests were used: unpaired Student's t test with Welch's correction, one-way ANOVA with Dunnett, Bonferroni or Fisher's LSD post-test, Two-way ANOVA with Dunnett or Bonferroni post-test. Sample sizes are indicated in figure legends and significance was defined as *$p < 0.05$, **$p < 0.01$, ***$p < 0.001$, ****$p < 0.0001$. NS = not significant.